small
methods

Supporting Information

for *Small Methods*, DOI 10.1002/smtd.202300647

Defect-Engineering by Solvent Mediated Mild Oxidation as a Tool to Induce Exchange Bias in Metal Doped Ferrites

Beatrice Muzzi, Martin Albino, Michele Petrecca, Claudia Innocenti, César de Julián Fernández, Giovanni Bertoni, M. Ricardo Ibarra, Mogens Christensen, Maxim Avdeev, Clara Marquina and Claudio Sangregorio**

Supporting information

Defect-engineering by solvent mediated mild oxidation as a tool to induce exchange bias in metal doped ferrites.

Beatrice Muzzi,[a,b,c] Martin Albino,[c] Michele Petrecca,[c] Claudia Innocenti,[b,c] César de Julián Fernández,[d] Giovanni Bertoni,[e] M. Ricardo Ibarra, [f, g, h] Mogens Christensen,[l] Maxim Avdeed,[m] Clara Marquina, [f, g,] Claudio Sangregorio[b,c,*]*

1. High-Resolution Transmission Electron Microscopy (HRTEM)

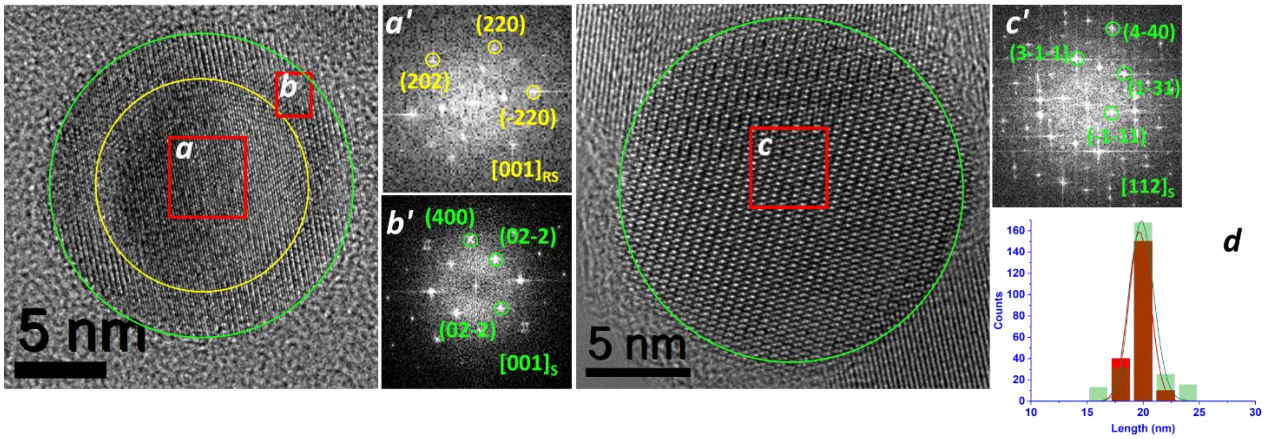

Figure S1. Left: HRTEM image of **FeO** with core@shell structure: the two red squares indicates the regions selected to identify the core (*a*) and the ca. 2 nm thick shell (*b*); FFT analysis of the selected regions: the labelled spots are related to crystallographic planes indexed as (*a'*) rock-salt phase ($\boldsymbol{Fm\bar{3}m}$), in zone axis $[001]_{RS}$ and (*b'*) cubic spinel structure ($\boldsymbol{Fd\bar{3}m}$), $[001]_S$. Right: HRTEM image of **FeO-oxy**: the core@shell structure disappeared and the FFT analysis of region *c* revealed the presence of the cubic spinel structure ($\boldsymbol{Fd\bar{3}m}$), in zone axis $[112]_S$. *d*) Size distribution of NPs before (**FeO**, green bars) and after (**FeO-oxy**, red bars) thermal annealing.

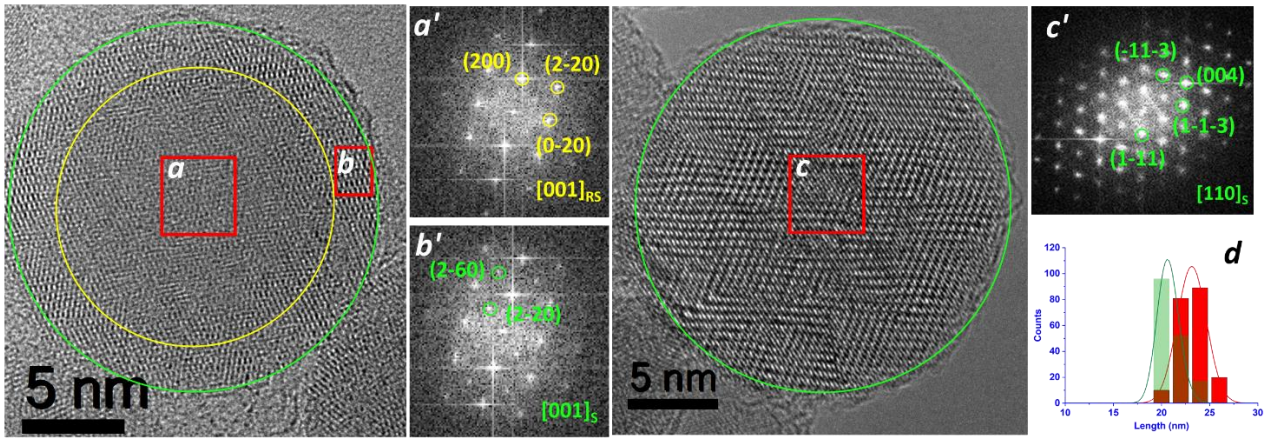

Figure S2. Left: HRTEM image of **CoFeO** with core@shell structure: the two red squares indicates the regions selected to identify the core (*a*) and the 2 nm thick shell (*b*); FFT analysis of the selected regions: the labelled spots are related to crystallographic planes indexed as (*a'*) rock-salt phase (***Fm$\bar{3}$m***), in zone axis $[001]_{RS}$ and (*b'*) cubic spinel structure (***Fd$\bar{3}$m***), $[001]_S$. Right: HRTEM image of **CoFeO-oxy**: the core@shell structure disappeared and the FFT analysis of region *c* revealed the presence of the cubic spinel structure (***Fd$\bar{3}$m***), in zone axis $[110]_S$. *d*) Size distribution of NPs before (**CoFeO**, green bars) and after (**CoFeO-oxy,** red bars) thermal annealing.

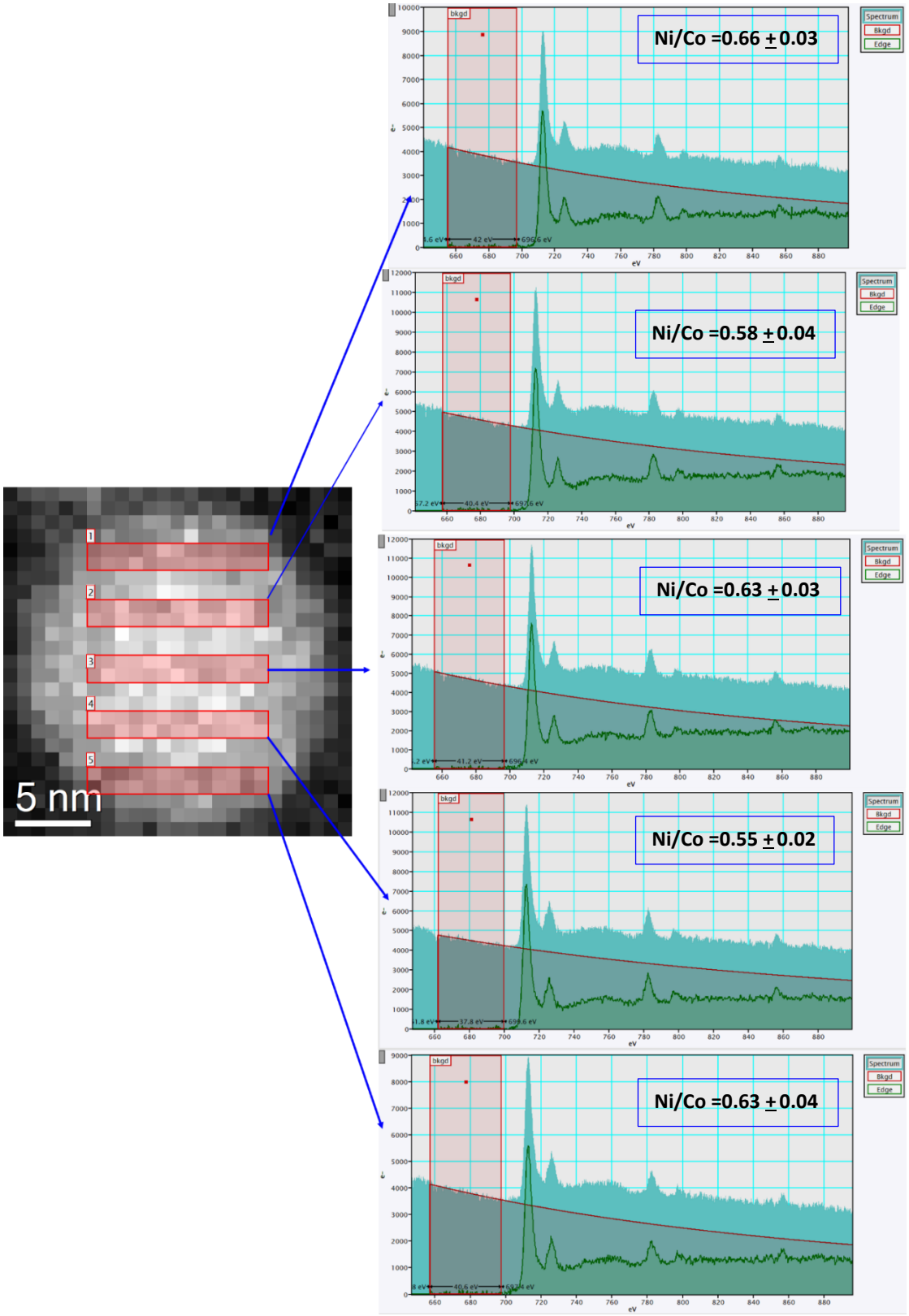

Figure S3. Left: EELS map of **NiCoFeO-oxy**; Right: EELS spectra related to different NP's regions. This analysis clearly demonstrates that, within the experimental error, no composition gradient for Ni and Co occurs within the NP. The same results were obtained by repeating the analysis over 5 NPs.

2. Powder X-ray diffraction and Neutron powder diffraction

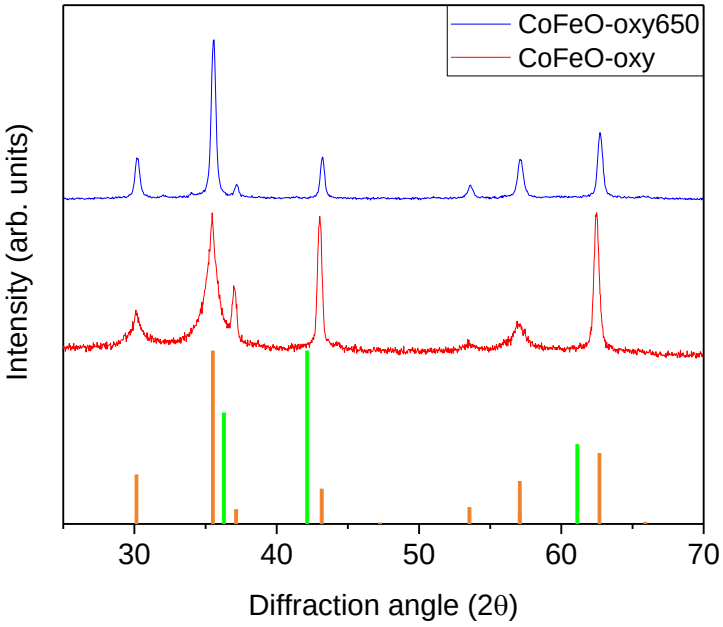

Figure S4. X-Ray diffraction patterns of **CoFeO-oxy** before (red pattern) and after (**CoFeO-oxy650**) (blue pattern) heating treatment at higher temperature (650 °C for 30 minutes in an oven); orange and green bars correspond to the reference pattern for Fe_3O_4 (JCPDS PDF #*19-0629*) and FeO (JCPDS PDF #*73-2144*), respectively.

The diffraction pattern of **CoFeO-oxy** and **CoFeO-oxy650** were recorded with a high intensity X-ray CoK_α source and with a neutron source. The powder diffraction patterns, reported in Figure 7 main text, displayed that both samples are single phase, within the instrumental resolution, and can be described as spinel ferrite (space group *Fm*-3*d*). The most striking difference between the powder diffraction patterns is the high background in the neutron powder diffraction pattern of the **CoFeO-oxy** sample, due the incoherent scattering of hydrogen of the surfactant (25% w/w) used for the solvent mediated oxidation. A second feature is the large difference in the peak width observed for some of the reflections in **CoFeO-oxy**. At close inspection of the neutron powder diffraction pattern, it is possible to discern weak peaks from the aluminium foil used for holding the samples. Combined Rietveld refinements of the neutron and CoK_α X-ray powder diffraction patterns were carried out to create robust models. The models were to a large extent identical for **CoFeO-oxy** and **CoFeO-oxy650**; Chebychev polynomials with eight coefficients were used for refining the background of all four patterns along with 2θ zero point shift. The unit cell parameter for the X-ray and neutron pattern were constrained to be identical, while the neutron wavelength was refined. The crystal structure was refined as spinel ferrite in the space group *Fm*-3*d* with metal ions occupying the tetrahedral 8*a*(⅛,⅛,⅛) and octahedral 16*c*(0,0,0) sites, while oxygen was free to refine on 32*e*(*x*,*x*,*x*), where *x* is close to ¼. The thermal vibration parameter was refined as a single overall B_{iso} parameter constrained between the X-ray and neutron data. In **CoFeO-oxy** and in **CoFeO-oxy-650** the Co/Fe occupancies were refined so that the Co/Fe ratio was the same. The magnetic phase was described by introducing

sufficient symmetry operators, so that the scale factor of the crystal structure and the magnetic structure, and the Co/Fe occupancies on the *Td* and *Oh* sites could be constrained one to one between the magnetic phase and the crystal structure. The atomic dipolar magnetic moment was described making the tetrahedral and octahedral magnetic sublattice to be anti-parallel. In addition, the cobalt and iron moment ratio was constrained to 3:5 assuming Co^{2+} and Fe^{3+}, hereby neglecting the possibility of part of the iron being Fe^{2+} and the potential orbital moment of Cobalt.

The description of peak broadening is different for **CoFeO-oxy** and for **CoFeO-oxy650**. In **CoFeO-oxy** a single overall size parameter $Y_{overall}$ is used for describing the peak width of the very broad reflections and an additional size parameter Y_{hkl} is used to reduce the peak broadening of the reflections (*hkl*) = (222), (400), (440), (622), (444), (800), (662), (840) and (844). The narrow reflections are found at the positions of the diffraction peaks corresponding to the monoxide with half the unit cell a = 4.2032 Å at (*hkl*) (111), (200), (220), (311), (222), (400), (331), (420) and (422). In **CoFeO-oxy650** three spherical harmonics parameters are used to describe the shape of the crystallites: K_{00}, K_{41} and K_{61}. An overview of the refined parameters can be found in Table S1.

Table S1: Crystallographic parameters extracted from the constrained Rietveld refinement of the neutron and X-ray powder diffraction collected on the samples **CoFeO-oxy** and **CoFeO-oxy650**.

	CoFeO-oxy	**CoFeO-oxy650**
a (Å)	8.4060(3)	8.3866(1)
O 32*e*(*x*,*x*,*x*)	0.2492(4)	0.2451(2)
Occupancy		
CoTd (8*a*)	-	10.5(1.4)%
FeTd (8*a*)	86.5(5)%	89.5(1.4)%
CoOh (16c)	41.0(1)%	36.9(1.5)%
FeOh (16*c*)	59.2(3)%	63.1(1.5)%
Composition	$Co_{0.82(4)}Fe_{2.05(6)}O_4$	$Co_{0.84(3)}Fe_{2.16(3)}O_4$
$B_{overall}$ (Å^2)	1.10(4)	0.39(2)
$MM(Fe^{3+})$ (μ_B)	4.2(2)	4.61(6)
Size		
$Y_{overall}$ / K_{00}	2.14(1)	3.60(2)
Y_{hkl} / K_{41}	-1.76(1)	-0.69(6)
- / K_{61}		0.58(5)
Size (nm)	17(1)	27(3)
R_F(Neutron)	4.95%	2.16%
R_{mag}(Neutron)	7.61%	3.51%
R_F(X-ray)	1.74%	1.84%
R_{wp}(Neutron)	1.89%	5.60%
R_{wp}(X-ray)	8.14%	9.89%
Parameters	34(18)/3	35(18)/3

Table S1 reports parameters extracted from the constrained Rietveld refinement of the neutron and CoK_α X-ray, recorded with a high intensity source, diffraction patterns collected on the samples **CoFeO-oxy** and **CoFeO-oxy650**. The atomic magnetic dipole moment (MM) is given for Fe^{3+}, it is assumed that the Co^{2+} moment is 3/5 of $MM(Fe^{3+})$. In total 34 and 35 parameters were refined in the two cases, 18 parameters are background and 2θ zero point, while 3 parameters are scale, unit cell and B_{iso} for the aluminium used as sample holder. The size parameter is extracted from the narrow

peaks in **CoFeO-oxy** and it is the average values based on the spherical harmonics refinement in the **CoFeO-oxy650** model. The R_{wp} values in the table is given without background correction, due to the large background in the **CoFeO-oxy** sample.

The model used for **CoFeO-oxy** is not completely describing the peak shape, especially a shoulder to the right hand side of the (111) reflection. The origin of the mismatch can be stacking faults or micro strain, both resulting in a deviation from the ideal lattice plane separation. Strain is expected to have a $X\tan\theta$ dependence, and different strain models have been attempted to describe the data, but without satisfying results. Stacking faults can be introduced, by disorder in the occupation of the *Td* site. The monoxide $Co_XFe_{1-X}O$ structure has cubic closed packing of the oxygen atoms with the transition metal ions occupying all *Oh* sites. In the spinel structure metal ions occupy ½ the *Oh* sites and only ⅛ of the *Td* site. The model used for the Rietveld refinement does not contain any local information regarding stacking faults or strain; however, the model describes the data very well and it can be assumed that the space average structure is well described. The peaks in the neutron and X-ray diffraction pattern are described using only two profile parameters, Y_{total} and Y_{hkl}, the sum Y_{total} + Y_{hkl} is used to extract the size of 17(1) nm. In **CoFeO-oxy650** a three parameters spherical harmonic model has been used to describe average sized crystallites of 27(1) nm. The spherical harmonics suggests the shape to be octahedrons with the (111) direction being truncated. The larger unit cell dimension of **CoFeO-oxy**, 8.4061(3) Å, can be due to electronegative repulsion from the oxygen atoms, as 14% cation are missing in the *Td* site. Interestingly the atomic magnetic dipole moment is comparable for the two samples with values of 4.3(1) and 4.61(6) μ_B for **CoFeO-oxy** and **CoFeO-oxy650**, respectively. A recent comprehensive study on $CoFe_2O_4$ gave also comparable moment at room temperature of 3.8-4.1 μ_B.

3. Energy Dispersive X-Ray Fluorescence (EDXRF)

Table S2. Iron, cobalt and nickel atomic percentage obtained by Energy Dispersive X-Ray Fluorescence (EDXRF) for **CoFeO-oxy** and **NiCoFeO-oxy.**

Samples	Fe (atomic %)	Co (atomic %)	Ni (atomic %)
CoFeO-oxy	69	31	-
CoFeO-oxy650	67	33	-
NiCoFeO-oxy	58	15	27

4. Magnetic measurements

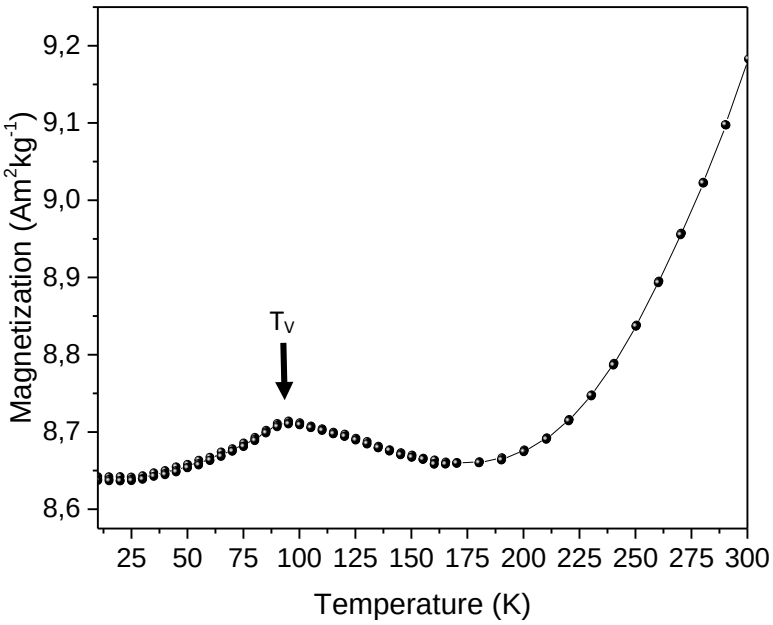

Figure S5. Temperature dependence of the magnetization of **FeO-oxy** after a FC procedure, applying a static field of 5 mT. Arrow points to T_V, corresponding to the Verwey transition characteristic of Fe_3O_4

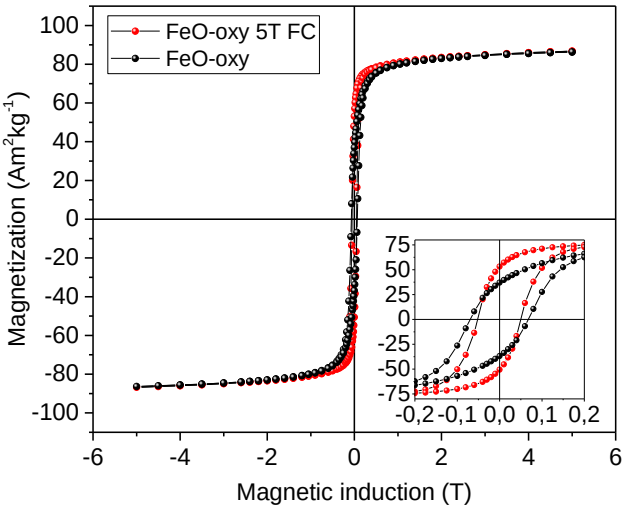

Figure S6. Hysteresis loops for **FeO-oxy** at 5 K after ZFC and FC (in 5 T applied magnetic field) procedures. The inset shows the low field regions.

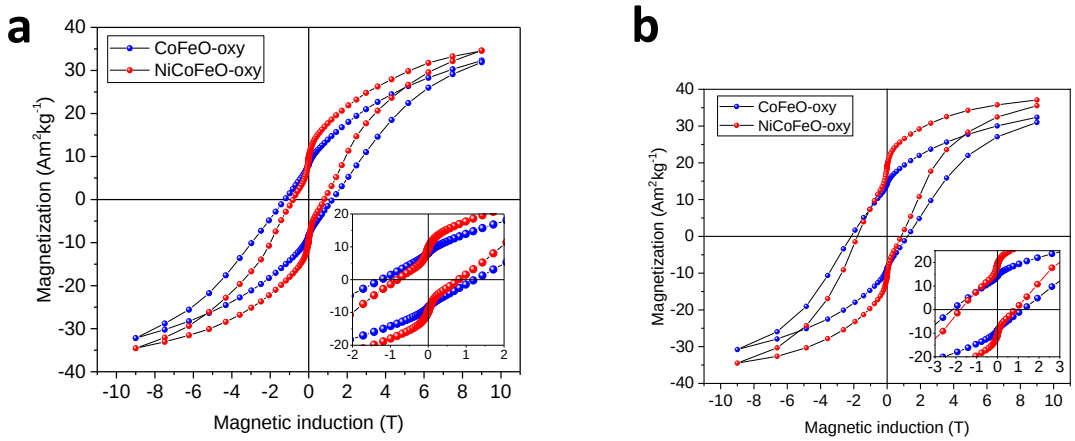

Figure S7. a) Hysteresis loops recorded at 5 K applying a 9 T magnetic field for the samples **CoFeO-oxy** and **NiCoFeO-oxy**; b) Hysteresis loops at 5 K after FC in a 9 T applied magnetic field. The insets show the low field regions. Blue: **CoFeO-oxy** and red: **NiCoFeO-oxy**

Hysteresis loops at 9T were measured after ZFC and FC procedures for the samples **CoFeO-oxy** and **NiCoFeO-oxy** (Figure S7*a* and *b*) with the aim to elucidate the minor loop contribution which can affect the H_E value. In both cases the loops are more symmetric than those obtained when applying 5 T, confirming that the hysteresis observed at 5T after FC was partially affected by a minor loop contribution. Indeed, the H_E observed for **CoFeO-oxy** and **NiCoFeO-oxy** after 9 T FC decreased to 0.48 and 0.5 T, respectively. Moreover, the two loops present a kink at remanence (H = 0 T) that can be attributed to the lattice strain defects (e.g. antiphase boundaries) that still occur in the oxidized NPs.

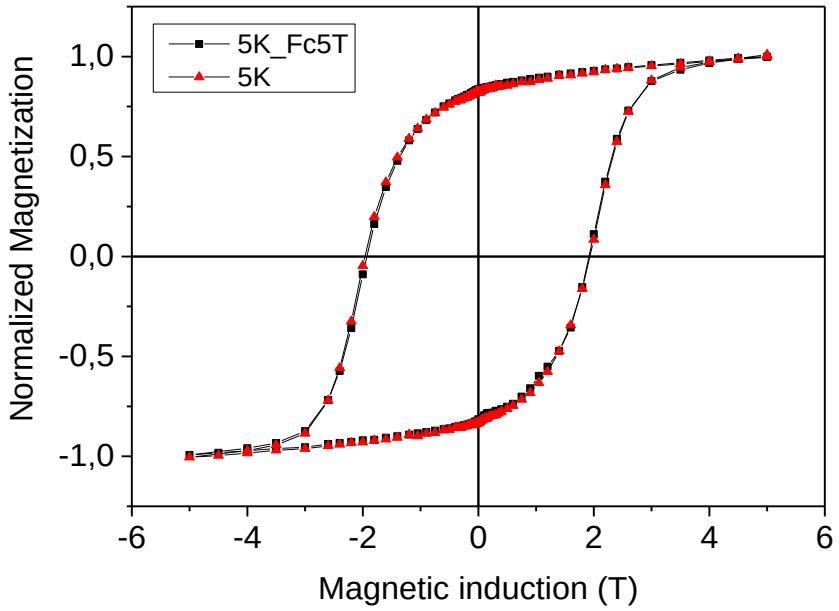

Figure S8. Hysteresis loops for **CoFeO-oxy650** at 5 K (red symbols) after ZFC and FC (in 5 T applied magnetic field) procedures.

$Ni_{0.53}Co_{0.40}Fe_{2.07}O_4$ synthetized by one-pot thermal decomposition of metal acetyl acetonate precursor (NiCo-ferrite)

Table S3. Structural Properties and chemical composition

Label	Stoichiometry	x[a]	y[a]	z[a]	% surf[b]	d XRD (nm)	d TEM (nm)	*a*
1a	$Ni_{0.53}Co_{0.40}Fe_{2.07}O_4$	0.40	0.53	2.07	19.2	5.6	5.95±0.94	8.372

[a] From ICP; [b] From CHN

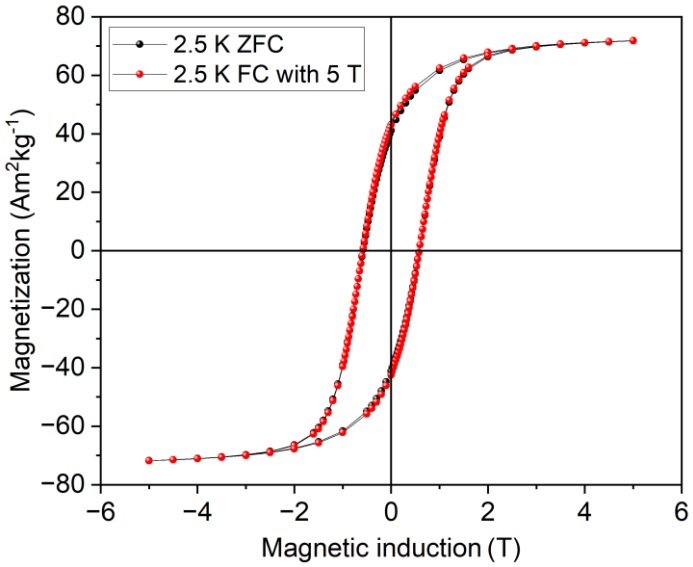

Figure S9. Hysteresis loops for **NiCo-ferrite** at 5 K (black symbols) after ZFC and FC (in 5 T applied magnetic field) procedures. The low temperature loop was recorded after ZFC and FC (5T) procedures; the two curves are superimposable.

Table S4. Magnetic Data on powder sample

Stoichiometry	T_{max}	H_C (T) 2.5 K	M_{5T} (Am^2kg^{-1}) 2.5K	M_R/M_{5T}	M_{5T} (Am^2kg^{-1}) 300K
$Ni_{0.53}Co_{0.40}Fe_{2.07}O_4$	110	0.58	72	0.59	57.92

Magnetic Data of core@shell $Fe_{0.95}O@Fe_3O_4$ (FeO), $Co_{0.3}Fe_{0.7}O@Co_{0.8}Fe_{2.2}O_4$ (CoFeO) and $Ni_{0.17}Co_{0.21}Fe_{0.62}O@Ni_{0.4}Co_{0.3}Fe_{2.3}O_4$ (NiCoFeO) NPs

Table S5. Magnetic data of core@shell NPs

Sample	5 K			300 K			5 K_FC 5 T			
	M_{5T} (Am^2kg^{-1})	M_R (R%) (Am^2kg^{-1})	μ_0H_C (T)	M_{5T} (Am^2kg^{-1})	M_R (R%) (Am^2kg^{-1})	μ_0H_C (T)	M_{5T} (Am^2kg^{-1})	M_R (R%) (Am^2kg^{-1})	$\mu_0H_C^{FC}$ (T)	μ_0H_E (T)
FeO	35	6 (17)	0.32	35	0.1 (0.3)	0.001	39	20 (51)	0.3	0.2
CoFeO	9	0.8 (9)	0.30	12	0.2 (2)	0.02	14	6 (43)	0.6	1.6
NiCoFeO	11	3 (30)	0.45	13	1 (8)	0.01	15	8 (53)	0.5	0.5

The Co,Ni doped core@shell NPs display an increased magnetic anisotropy with respect to the $Fe_{1-x}O@Fe_3O_4$ NPs, but a marked lower M_{5T}. This latter decrease is attributed to the magnetic disorder in the shell induced by the substitution of $Fe^{(II)}$ for $Co^{(II)}$, which prevents the formation of a well-defined S structure after the controlled mild passivation step. Thus, such disorder makes the relative contribution of the FiM component less important. Conversely, in **NiCoFeO,** $Ni^{(II)}$ restores the magnetic order in the ferrite shell, enhancing the magnetization at 5 T and the remanence values compared to **CoFeO** NPs.

Magnetization isotherms (not shown) clearly indicates that a strong exchange coupling is operating between the monoxide and the ferrite phases. Low temperature hysteresis loops, recorded after FC from 360 K with a 5 T magnetic field display the presence of EB (i.e., a loop-shift along the field axis) and an increase of the coercive field. Considering that the EB is turned on only when the NPs are FC across the Néel temperature of the AFM core, it can be reasonably assumed that the EB arises from the core@shell AFM@F(i)M interface and not from other mechanisms.

5. Morphology Characterization

FeO-oxy

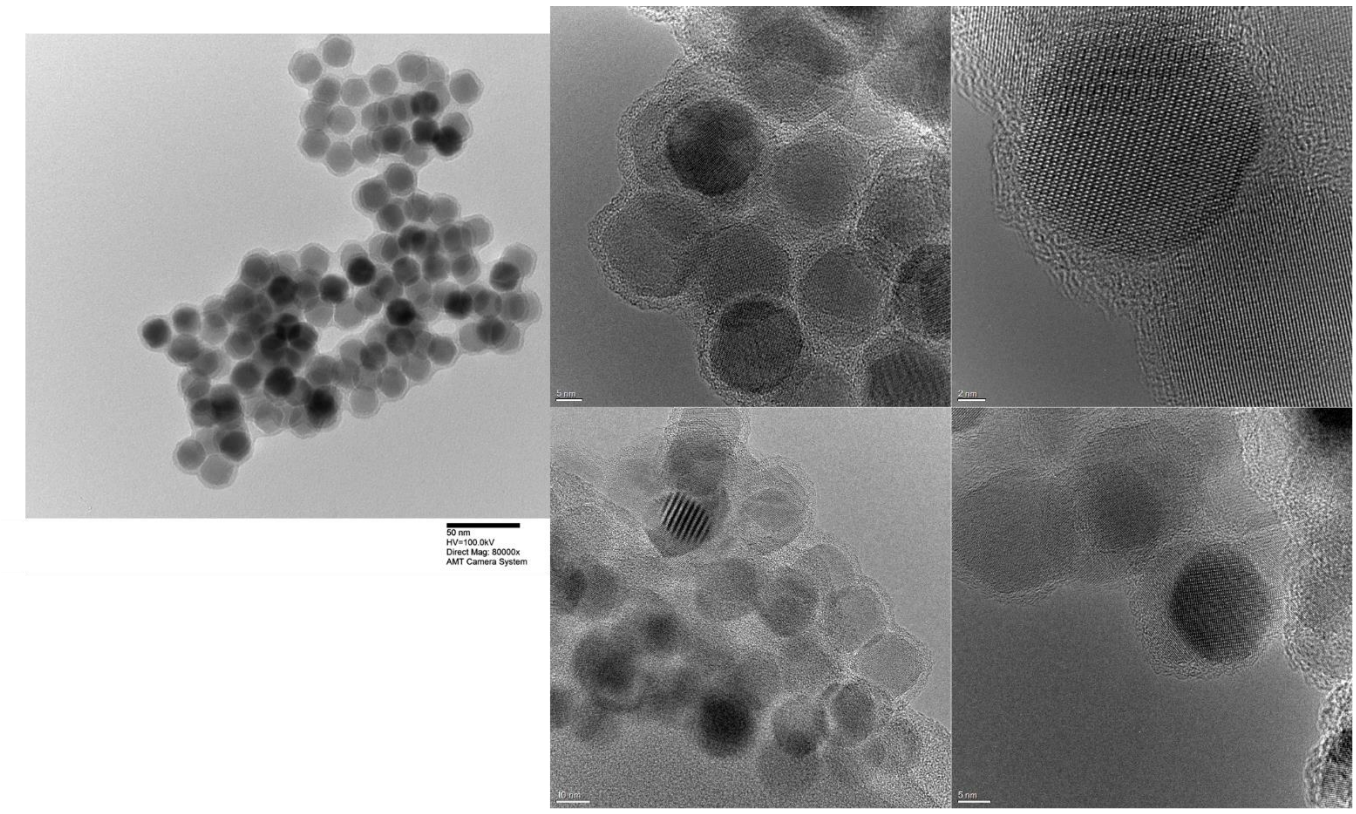

Figure S10. TEM and HRTEM images of **FeO-oxy.**

CoFeO-oxy

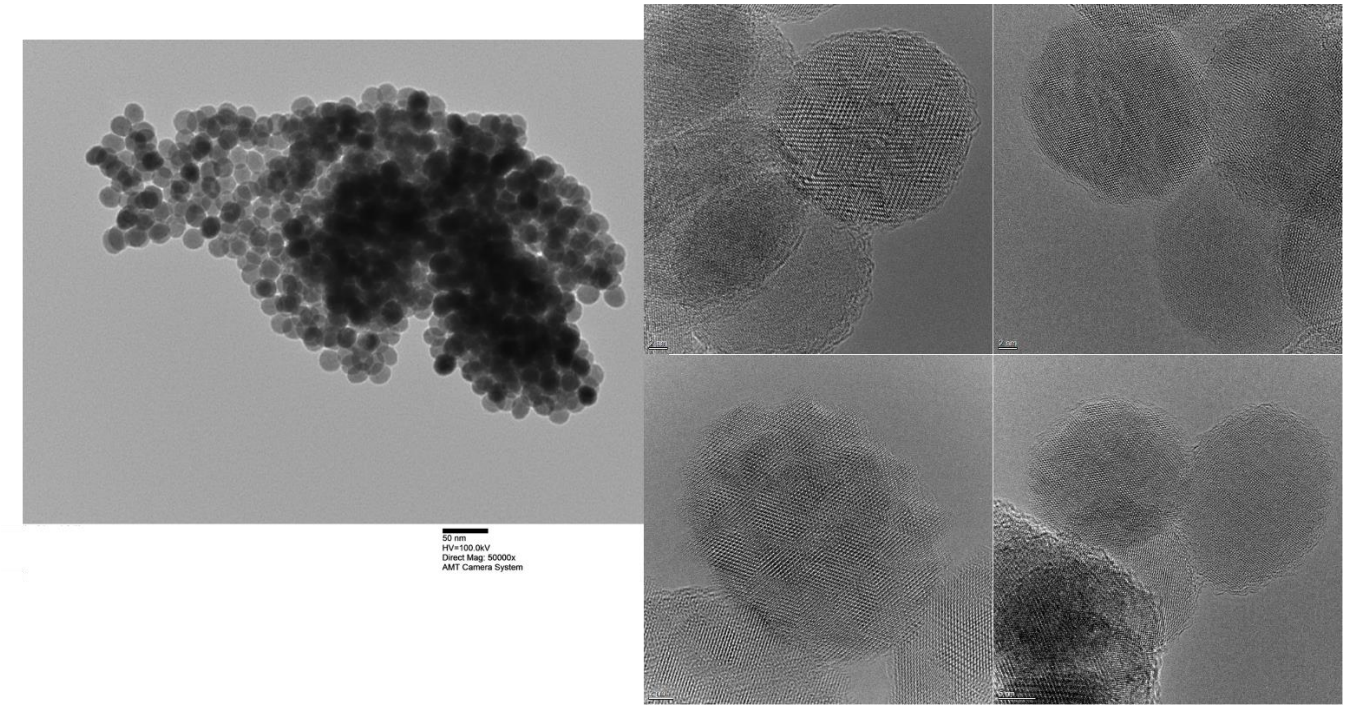

Figure S11. TEM and HRTEM images of **CoFeO-oxy.**

NiCoFeO-oxy

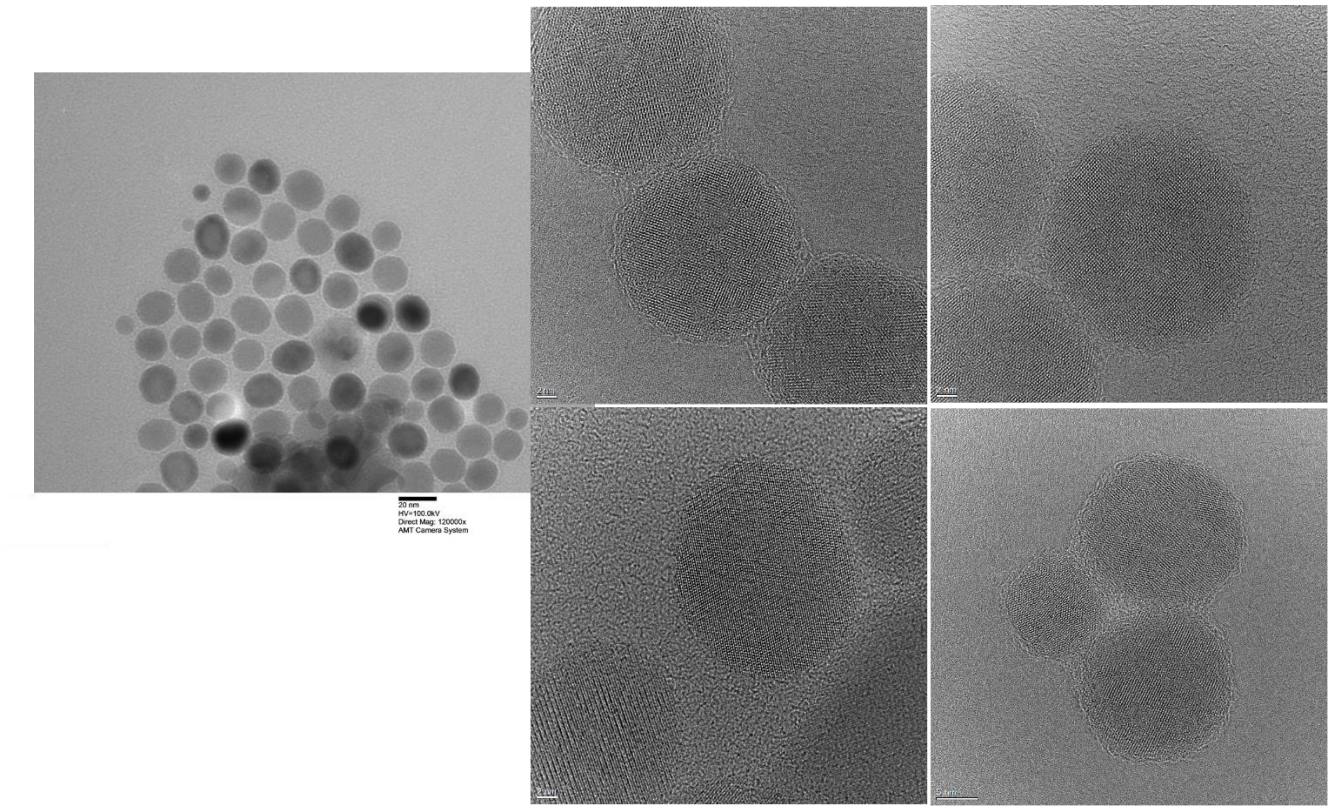

Figure S12. TEM and HRTEM images of **NiCoFeO-oxy.**